Human–AI Co-reasoning for Clinical Diagnosis with Evidence-Integrated Language Agent

Zhongzhen Huang[1†], Yan Ling[3†], Hong Chen[3†], Ye Feng[2], Li Wu[2], Linjie Mu[1], Shaoting Zhang[1,5], Xiaofan Zhang[1,4*], Kun Qian[5,6*], Xiaomu Li[2,3*]

[1]*Shanghai Jiao Tong University, Shanghai, China*

[2]*Department of Endocrinology, The First Affiliated Hospital, Zhejiang University School of Medicine, Hangzhou, China*

[3]*Department of Endocrinology, Zhongshan Hospital, Fudan University, Shanghai, China*

[4]*Shanghai Innovation Institute, Shanghai, China*

[5]*SenseTime, Shanghai, China*

[6]*Multimedia Laboratory, The Chinese University of Hong Kong, Hong Kong SAR, China*

†***Contributed Equally***

∗***Corresponding authors****: Xiaofan Zhang(xiaofan.zhang@sjtu.edu.cn), Kun Qian(kqian@cuhk.edu.hk), Xiaomu Li(li.xiaomu@zju.edu.cn)*

Abstract

We present PULSE, a medical reasoning agent that combines a domain-tuned large language model with scientific literature retrieval to support diagnostic decision-making in complex real-world cases. To evaluate its capabilities, we curated a benchmark of 82 authentic endocrinology case reports encompassing a broad spectrum of disease types and incidence levels. In controlled experiments, we compared PULSE's performance against physicians with varying levels of expertise—from residents to senior specialists—and examined how AI assistance influenced human diagnostic reasoning. PULSE attained expert-competitive accuracy, outperforming residents and junior specialists while matching senior specialist performance at both Top@1 and Top@4 thresholds. Unlike physicians, whose accuracy declined with disease rarity, PULSE maintained stable performance across incidence tiers. The agent also exhibited adaptive reasoning, increasing output length with case difficulty in a manner analogous to the longer deliberation observed among expert clinicians. When used collaboratively, PULSE enabled physicians to correct initial errors and broaden diagnostic hypotheses, but also introduced risks of automation bias. The study explores both serial and concurrent collaboration workflows, revealing that PULSE offers robust support across common and rare presentations. These findings underscore both the promise and the limitations of language model–based agents in clinical diagnosis, and offer a framework for evaluating their role in real-world decision-making.

Introduction

Accurate diagnosis is foundational to effective medical care, yet diagnostic error remains common and consequential [1–3]. Patients with atypical, multisystem, or low-incidence diseases often experience prolonged diagnostic journeys because early presentations are nonspecific and many clinicians encounter such conditions too infrequently to build rapid recognition [4,5]. Endocrinology exemplifies these challenges: endocrine disorders frequently present with subtle, overlapping symptom profiles and can masquerade as cardiovascular, neurological, or psychiatric conditions [6,7]. Interpretation is further complicated by interdependent biochemical abnormalities and heterogeneous phenotypes, which can inflate the differential diagnosis and demand iterative hypothesis refinement over time [8].

In practice, diagnostic performance depends not only on medical knowledge but also on structured reasoning frameworks and experience [9–11]. Expert physicians rely on well-developed cognitive scripts and pattern recognition to navigate uncertainty, often drawing from a broader and more structured repertoire of disease representations and differential hypotheses. In contrast, trainees and early-career physicians are more susceptible to common reasoning failures, such as premature closure, settling on an initial diagnosis before the full evidentiary picture is integrated [12]. Although medical education aims to bridge this gap, accumulating broad diagnostic exposure requires years of practice, leading to disparities in diagnostic quality across settings and regions. Meanwhile, endocrine science evolves rapidly, reinforcing the need for continuous learning and accessible expertise [13–15].

The rapid evolution of artificial intelligence (AI), particularly large language models (LLMs), offers a potential mechanism to democratize diagnostic support by enabling interactive, natural-language clinical reasoning [1]. Recent systems have shown promising performance on answering intricate clinical questions, synthesizing literature, and supporting decision-making. Notably, work such as AMIE reframes evaluation from single-shot diagnosis to the process of developing a differential diagnosis (DDx) through interaction, demonstrating that an LLM interface can improve the quality of clinician-generated DDx compared with conventional information retrieval tools [8]. At the same time, the emergence of reasoning models, such as OpenAI-o1 [16] and DeepSeek-R1 [17], marks a pivotal shift toward employing LLMs to solve complex tasks [18]. For instance, OpenAI-o1 has surpassed the passing threshold of the United States Medical Licensing Examination (USMLE) with scores approaching 95% [16]. When integrated with external tools for evidence retrieval, these systems offer a compelling opportunity to reimagine human-AI collaborative diagnosis and have the potential to improve both the timeliness of care delivery [12].

Despite growing enthusiasm, empirical evidence for human-AI collaborative diagnosis remains mixed [19]. Recent meta-analyses indicate that collaborative performance does not consistently exceed that of the best

individual agent, and in some instances, uncritical reliance on AI can degrade human performance [20].

Moreover, much of the existing literature focuses on narrowly defined tasks, such as radiological image classification [21], or simplified vignette-style text problems that lack longitudinal context [22]. These paradigms differ substantially from real-world diagnostic reasoning, which often involves high-level cognitive integration. As a result, it remains unclear how reasoning-oriented agents influence physician decision-making in complex, real-world cases. Furthermore, the optimal workflow for such collaboration is undefined. AI can function as a late-stage "second opinion," prompting physicians to review or revise their diagnosis, or as a real-time "co-pilot" that concurrently shapes the hypothesis space during the initial diagnostic process. These workflows impose different cognitive demands and may differentially affect diagnostic accuracy, efficiency, and susceptibility to over-reliance. However, rigorous head-to-head evaluations comparing these workflows across levels of physician experience remain comparatively sparse.

To address this unmet need, we design a structured experimental framework to elucidate the advantages of reasoning-based agents and to characterize the role of human–AI collaboration in complex diagnostic settings. We first introduce PULSE, a medical reasoning agent that integrates a reasoning-oriented LLM with a scientific literature retrieval engine to support diagnostic reasoning in challenging cases. We then curate a set of of 82 complex, real-world endocrinology case reports spanning multiple disease categories and incidence tiers, and benchmark PULSE against physicians across a spectrum of expertise, from residents to senior attending specialists. For human–AI collaboration, we explicitly compare two operational modes: serial collaboration (physicians diagnose independently, then review and revise with PULSE) and concurrent collaboration (physicians receive assistance during the initial diagnostic process).

In summary, we assess four clinically relevant dimensions of utility: (1) the performance of PULSE and individual physicians across the long tail of disease incidence; (2) the relationship between case difficulty and reasoning effort, quantified as diagnostic time for physicians and generation tokens for models; (3) the impact of AI assistance and different collaboration workflows on diagnostic outcomes. Across these evaluations, PULSE demonstrates expert-competitive performance consistently explores a broader diagnostic hypothesis space than individual physicians. AI support substantially elevates resident performance toward specialist levels. Together, these findings delineate when and how LLM-based reasoning agents can augment diagnostic reasoning in endocrinology, while underscoring the importance of collaboration workflow design and safeguards against over-reliance.

Results

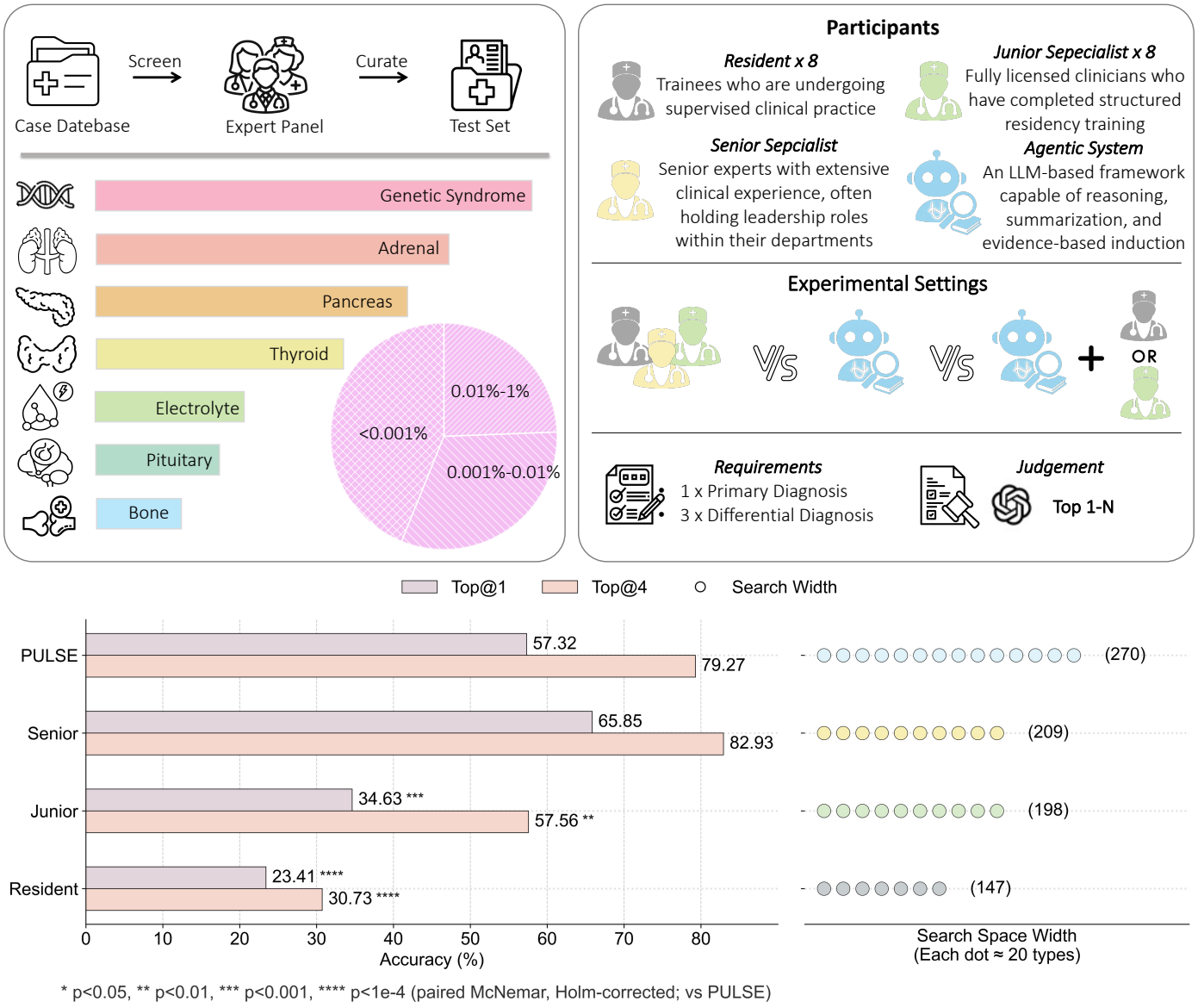

Figure 1: **Experiment settings and overall performance. Upper:** The PULSE agent was evaluated against physicians across three experience strata (Senior, Junior, and Resident) on these 82 endocrinology cases collected across seven subspecialty domains and stratified into three incidence categories based on disease prevalence. **Bottom left:** Diagnostic accuracy quantified by Top@1 (purple) and Top@4 (pink). Asterisks indicate statistical significance compared to PULSE ($*P < 0.05$, $**P < 0.01$, $***P < 0.001$, $****P < 1 \times 10^{-4}$; paired McNemar test, Holm-corrected). **Bottom right:** Breadth of diagnostic hypotheses (Search Space Width).

Settings We evaluated the proposed medical reasoning agent (PULSE) on 82 diagnostically challenging endocrinology cases and benchmarked it against physician groups spanning three experience strata: one senior specialist, eight junior specialists, and eight residents (Figure 1). The 82 cases were collected across seven endocrinology subspecialty domains: hereditary syndrome-related disorders, adrenal diseases, pancreatic endocrine diseases, pituitary diseases, thyroid and parathyroid diseases, electrolyte disorders, and bone and joint diseases. These cases are stratified into three incidence categories (0.01–1%, 0.001–0.01%, and $< 0.001\%$). Each case included detailed clinical presentations, laboratory findings, imaging data, and pathological infor-

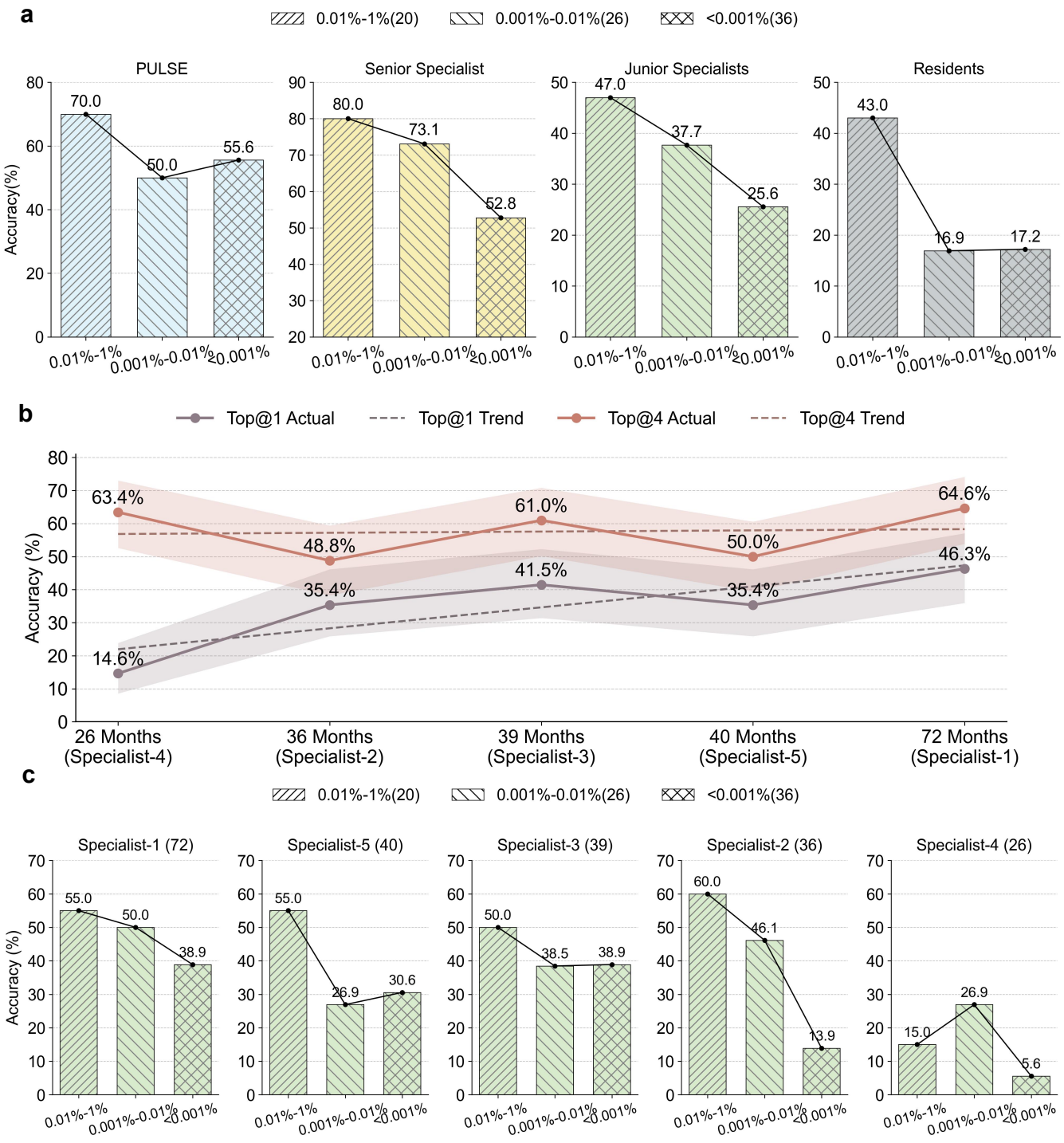

Figure 2: **a**, Comparison of diagnostic accuracy stratified by three disease incidence tiers (0.01–1%, 0.001–0.01%, and <0.001%) for PULSE, the senior specialist, pooled junior specialists ($n = 5$), and pooled residents ($n = 5$). **b**, Top@1 and Top@4 accuracy of individual junior specialists plotted against their clinical experience in months. Points show observed accuracy, shaded band indicates 95% Wilson confidence intervals, dashed line denotes the linear trend across individuals. **c**, Granular analysis of diagnostic accuracy across incidence tiers for individual junior specialists, annotated with their cumulative clinical experience in months.

mation, with a reference diagnosis established through expert consensus serving as the gold standard.

For each case, participants independently provided one primary diagnosis and three differential diagnoses (Upper part of Figure 1). We employed GPT-5.1 [23] as an automated evaluation tool to assess the semantic consistency between the diagnoses provided by each participant and PULSE against the reference diagnosis, thereby reducing subjective bias in manual adjudication and improving the efficiency and reproducibility of the evaluation process. Performance was quantified as Top@1 (primary diagnosis matches the reference) and Top@4 (reference appears anywhere within the four provided diagnoses).

Performance overview Across cases, PULSE demonstrated consistently strong diagnostic performance, exceeding that of less-experienced physicians and approaching senior-specialist level (lower part of Figure 1). At Top@1, PULSE achieved an accuracy of 57.32%, substantially exceeding junior specialists (34.63%) and residents (23.41%). These differences were statistically significant under case-level paired McNemar tests using a conservative majority-vote definition for physician groups (junior specialists: $p = 7.8 \times 10^{-5}$, Holm-corrected $p = 1.6 \times 10^{-4}$; residents: $p = 2.0 \times 10^{-6}$, Holm-corrected $p = 5.0 \times 10^{-6}$). In contrast, while the senior specialist achieved a higher Top@1 accuracy (65.85%) than PULSE, this 8.5-point difference was not statistically significant ($p = 0.25$), indicating comparable top-ranked diagnostic performance. At Top@4, PULSE reached 79.27%, closely matching the senior specialist (82.93%), with no statistically significant difference observed (exact McNemar $p = 0.58$). This pattern suggests that the agent's primary prioritization modestly trails expert-level specificity, whereas its short-list differential coverage is statistically indistinguishable from that of a senior endocrinologist. By comparison, junior specialists (57.56%) and residents (30.73%) remained substantially lower, and the performance gaps relative to PULSE were again statistically significant (junior specialists: $p = 4.1 \times 10^{-3}$, Holm-corrected $p = 8.1 \times 10^{-3}$; residents: $p = 1.1 \times 10^{-8}$, Holm-corrected $p = 3.3 \times 10^{-8}$). Collectively, these paired performance-significance comparisons indicate that PULSE consistently and significantly outperforms less-experienced physician groups, while differences relative to the senior specialist are small and statistically non-significant.

Breadth of diagnostic hypotheses Diagnosis can be viewed as a process of expanding and subsequently narrowing a hypothesis space. With increasing clinical experience, physicians accumulate exposure to a broader range of disease entities, which enlarge the set of conditions considered during assessment. Consistent with this view, the total number of distinct diagnoses generated across cases increased with physician seniority (Figure 1). Senior specialist considered a mean of 209.0 distinct disease entities, followed by junior specialists (198.2) and residents (147.8). This gradient suggests that clinical tenure is associated with a progressively broader diagnostic search space. In contrast, PULSE generated 270 distinct disease entities, exceeding all individual physician groups, indicating a consistently expansive hypothesis space irrespective of experience constraints. This observation raises a clinically relevant question: whether a broader hypothesis space translates into greater robustness, particularly in conditions that fall outside routine clinical exposure.

Accuracy across disease incidence tiers Clinical experience is inherently shaped by disease frequency for humans, with common conditions encountered far more frequently than rare ones during medical training and practice. As a result, disease incidence represents a natural axis along which diagnostic difficulty and experience-related variability may emerge. Motivated by this consideration, we examined how diagnostic performance varies across disease incidence tiers and compared the proposed agent with physician groups (Figure 2a). Across physician groups, diagnostic performance showed a clear dependence on disease incidence. In particular, junior specialists exhibited a significant decline in accuracy as incidence decreased (odds ratio [OR] per tier $= 0.69$, $p = 0.038$), with performance dropping to 25.6% in the ultra-rare stratum ($< 0.001\%$). Experience-related disparities were most pronounced in this ultra-rare tier, where junior specialists and residents performed substantially worse than the senior specialist, with significantly reduced odds of a correct diagnosis (junior specialists: OR $= 0.31$, $p < 0.001$; residents: OR $= 0.21$, $p < 0.001$). In contrast, PULSE exhibited no significant incidence-dependent trend in diagnostic accuracy (OR per tier $= 0.78$, $p = 0.376$), maintaining relatively stable performance across all incidence strata. The absence of a monotonic performance decay suggests that the agent is comparatively insensitive to disease rarity, demonstrating its potential to mitigate experience-dependent diagnostic degradation in the long tail of rare diseases.

To further probe the role of clinical tenure, we analyzed variability within the junior-specialist cohort (Figure 2b, c), representing a period of rapid professional development. Within this group, diagnostic accuracy increased with months of practice, though with notable inter-individual variability. Notably, incidence-stratified analyses revealed the same qualitative pattern observed at the group level: performance was relatively stable in higher-incidence tiers but diverged sharply in the ultra-rare stratum. Even increased experience did not uniformly protect against performance loss in the rarest cases.

Experience-dependent accuracy patterns While the broad categorization of physicians into three groups captures macro-level differences, it may mask the fine-grained impact of clinical tenure. To contextualize this trend, we next examined performance variability within the junior specialist cohort. Within the junior specialist group, performance was positively associated with clinical experience, though with notable inter-individual variability (Figure 2c). The most experienced junior specialist (72 months) achieved the highest Top@1 (46.34%; 95% CI 35.96–57.06), while mid-experience specialists (36–40 months) clustered between 35.37% and 41.46%. However, a distinct dissociation between retrieval and prioritization was observed in Specialist 4 (26 months), who exhibited low Top@1 (14.63%) but robust Top@4 (63.41%).This profile implies that less experienced physicians may successfully retrieve candidate diagnoses but lack the reasoning structure to prioritize them effectively—a limitation the agent appears to circumvent through structured evidence weighting.

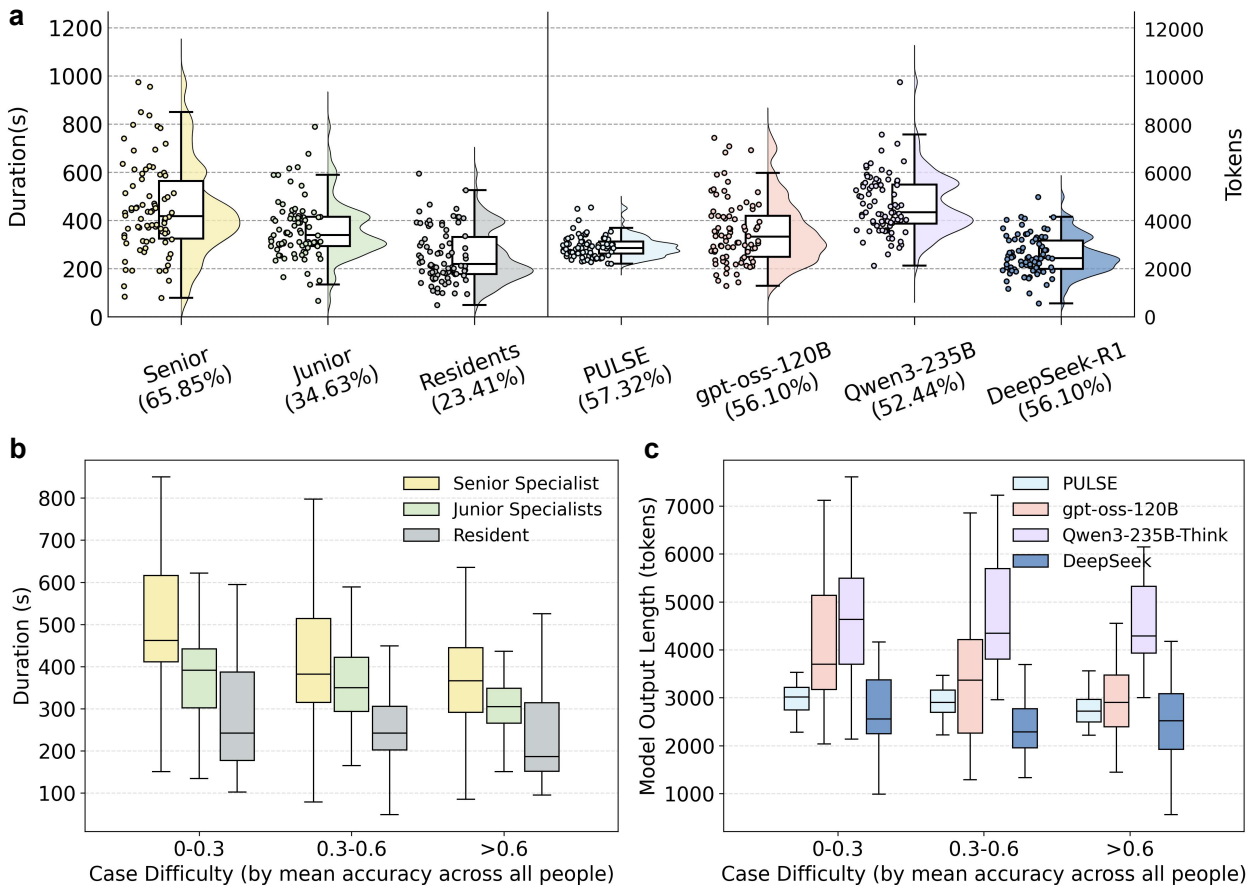

Figure 3: **a**, Distributions of per-case diagnostic time for physicians (left y-axis; residents, junior specialists, senior specialists) and per-case model deliberation measured as output length in tokens (right y-axis; PULSE, gpt-oss-120B, Qwen3-235B, DeepSeek-R1). Points denote individual cases; boxplots show median and interquartile range; half-violins depict kernel density. **b**, Physician diagnostic time stratified by case difficulty, defined by bins of mean diagnostic accuracy across all participants (0–0.3, 0.3–0.6, >0.6). Boxplots summarize case-level times within each difficulty bin and experience group. **c**, Model output length (tokens) stratified by the same difficulty bins.

Deliberation patterns and adaptive effort allocation Accurate diagnosis often requires sustained reasoning effort. Beyond diagnostic accuracy, we therefore examined how both human physicians and models allocate deliberation across cases, using diagnostic time as a proxy for human effort and output length as a proxy for model-side reasoning intensity.

Among physicians, diagnostic duration increased systematically with experience level (Figure 3a). The senior specialist spent the most time per case (mean 445.52 ± 191.45, s), followed by junior specialists (378.07 ± 211.06, s) and residents (253.58 ± 111.63, s). To assess whether physicians modulated deliberation effort in response to case difficulty, we stratified diagnostic time by bins of mean case-level accuracy across participants (0–0.3, 0.3–0.6, and > 0.6) and tested monotonic trends using Spearman correlation. Crucially, experts modulated their effort based on difficulty. Senior specialists ($\rho = -0.311$, $P = 0.0044$) and junior specialists ($\rho = -0.271$, $P = 0.0139$) exhibited a significant adaptive response, spending progres-

sively more time on cases with lower overall accuracy (Figure 3b). In contrast, residents exhibited a weaker, non-significant association ($\rho = -0.171$, $P = 0.125$), indicating reduced sensitivity of time investment to escalating case difficulty in the least experienced group. These findings indicate that expert performance in complex endocrinology is characterized by deliberate, extended reasoning, whereas less experienced physicians may reach premature closure. We then examined whether analogous patterns were present in models by quantifying reasoning intensity via output length (Figure 3c). Notably, high-performing models like PULSE ($\rho = -0.255, P = 0.0207$) and gpt-oss-120B [24] ($\rho = -0.367, P = 6.9 \times 10^{-4}$) displayed an "adaptive thinking" profile similar to senior physicians, where they significantly increased reasoning time for more difficult cases. In contrast, no significant trend was detected for Qwen3-235B-Thinking [25] ($\rho = -0.025, P = 0.826$) or DeepSeek-R1 ($\rho = -0.096, P = 0.391$). Together, these results highlight that adaptive allocation of reasoning effort is a potentially important mechanistic correlate of high-quality medical reasoning in complex diagnostic settings.

Human-AI Collaborative Performance While prior analyses suggest that PULSE shares several mechanistic features with expert-level reasoning, its clinical relevance ultimately depends on whether these capabilities translate into improved human decision-making under collaboration. To assess this, we evaluated the agent in a collaborative setting in which five junior specialists re-diagnosed cases after reviewing the agent's output (Figure 4a). Across all junior specialists, collaboration with PULSE led to consistent improvements in diagnostic accuracy.

In addition to overall performance changes, we examined how physicians selectively interacted with the agent's suggestions by analyzing asymmetric discordance patterns observed during re-diagnosis (Figure 4b). We characterized how physicians responded to AI advice, summarizing the trade-off between response to *Change* (correction vs. misleading rates) and *Persistence* (stability vs. inefficacy). We analyzed physician responses in cases where initial diagnoses differed from the agent's suggestions (*Change*). In scenarios where physicians were initially incorrect, AI assistance frequently triggered beneficial revisions, with correction rates ranging from 35.4% to 47.2% across individuals. At the same time, physicians occasionally adopted incorrect AI suggestions when their initial diagnoses were correct, indicating susceptibility to misleading advice. Importantly, for all attendings, corrective effects outweighed detrimental switching, resulting in a of cases, highlighting a residual inertia that limited the full corrective potential of AI assistance. Ultimately, despite the susceptibility to being misled and the persistence of certain errors, net benefit remained positive for all specialists. This indicates that persistence more often protected correct decisions than entrenched incorrect ones, albeit with notable inter-individual variability.

We next examined whether collaborative gains varied by disease incidence. Stratifying assisted performance across the same three incidence tiers (Figure 5), we observed that AI collaboration attenuated the

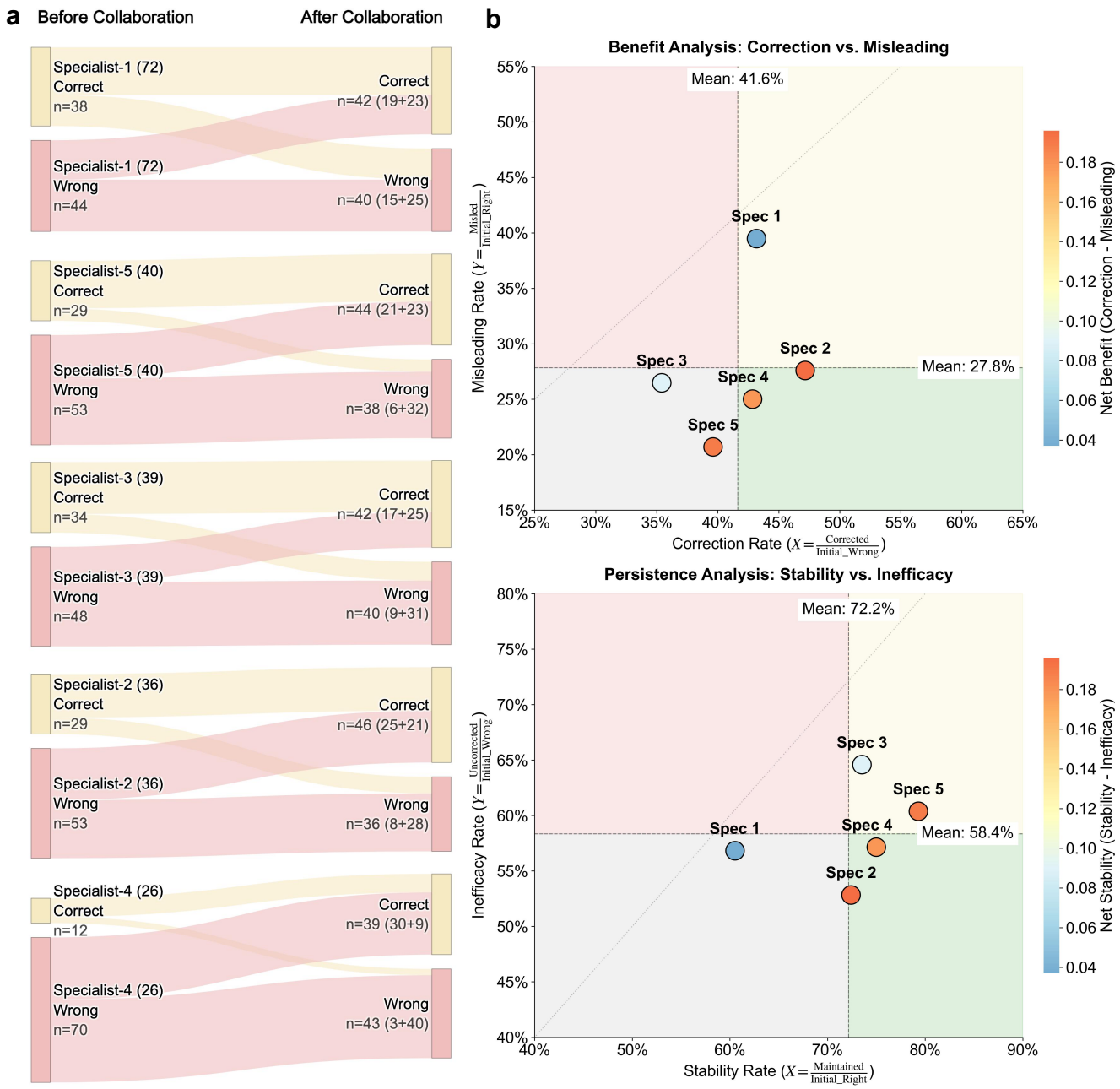

Figure 4: **a**, Sankey diagrams showing how five junior specialists' diagnostic decisions transitioned before and after reviewing the agent's output. Flows track the transitions between correct (yellow) and incorrect (red) diagnoses for each specialist. Node widths and link thicknesses are proportional to case counts, illustrating heterogeneous yet consistently positive net gains across physicians. **b**, Quantitative characterization of collaboration trade-offs. Top panel plots *Correction rate* (fraction of initially wrong diagnoses corrected after AI assistance) against *Misleading rate* (fraction of initially correct diagnoses overturned incorrectly), with point color indicating net benefit (correction minus misleading). Bottom panel plots *Stability rate* (retention of correct initial diagnoses) against *Inefficacy rate* (retention of incorrect initial diagnoses), with color indicating net stability (stability minus inefficacy). Dashed lines denote cohort means, and shaded quadrants highlight favorable (high correction or stability with low misleading or inefficacy) versus unfavorable regimes.

incidence-dependent decay seen in unassisted analyses. In the relatively common rare-disease tier (0.01–1%), collaboration yielded universal improvements, with absolute gains ranging from +10.0 to +35.0 percentage

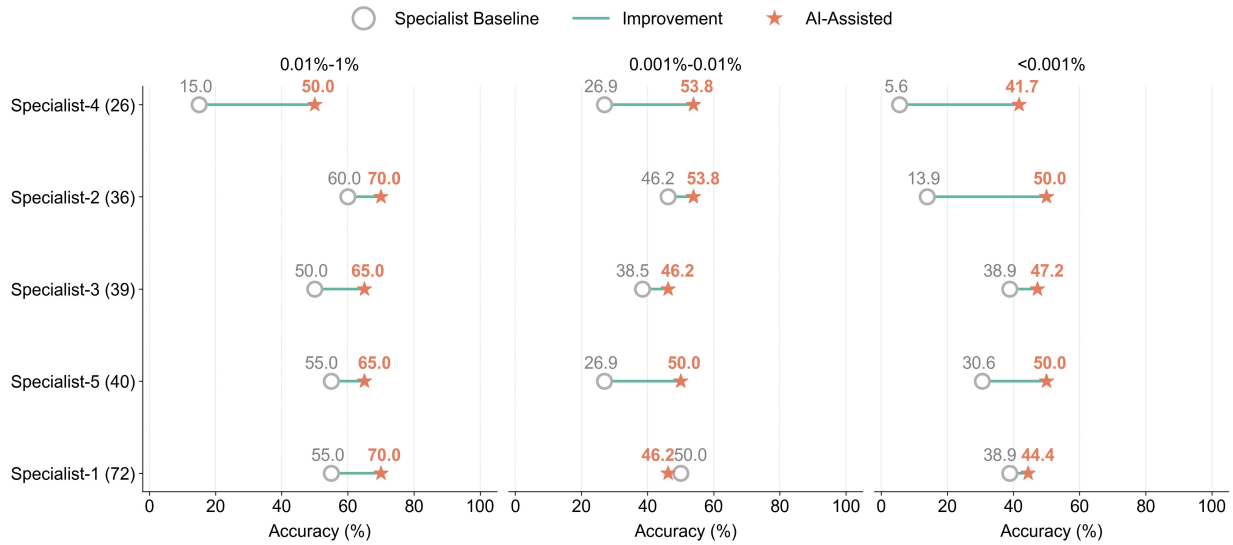

Figure 5: Impact of AI assistance stratified by disease incidence. Dumbbell plots track the absolute change in diagnostic accuracy for five junior specialists across three rarity tiers. Hollow circles represent unassisted baseline performance, and solid stars indicate AI-assisted performance. Lines connect within-physician changes (green for improvement, red for decline).

points. Gains remained consistently positive in the intermediate tier (0.001–0.01%). The most pronounced restorative effect occurred in the ultra-rare stratum ($< 0.001\%$), where baseline performance had been lowest. Here, AI-assisted accuracies converged into a relatively narrow band (46.67%–50.00%) despite wide disparities in unassisted performance. These findings indicate that collaboration functions as a stabilizing equalizer, particularly in the long tail of rare diseases where human-only diagnostic accuracy is most fragile.

Mechanisms of collaboration: serial versus concurrent workflows Building on the preceding analyses of human decision dynamics of reviewing AI outcomes, we next sought to probe how different collaboration workflows influence decision-making. Specifically, we compared two distinct collaboration workflows that differ in whether AI input is incorporated after or during human diagnostic reasoning. In the serial collaboration setting, corresponding to Junior Specialists 1–5 analyzed above, physicians first arrived at an independent diagnosis and subsequently reviewed the agent's suggestions, allowing AI input to function primarily as a post-hoc corrective signal. In contrast, the concurrent collaboration setting involved an additional cohort of three junior specialists and three residents (Specialists 6–8 and Residents 1–3), who had access to AI outputs simultaneously with case materials, effectively functioning as a real-time "co-pilot".

Across both collaboration modes, diagnostic accuracy improved substantially compared to the unassisted baseline (Figure 6a). In the serial group, Top@1 accuracies ranged from 47.6% to 56.1%, with Top@4 accuracies between 67.1% and 75.6%. The concurrent collaboration group achieved comparable performance, and in some cases outperformed the serial group. Specialists 6–8 operating in concurrent mode recorded Top@1 accuracies of 45.1% to 59.8%. Most strikingly, residents using the AI concurrently—who had significantly

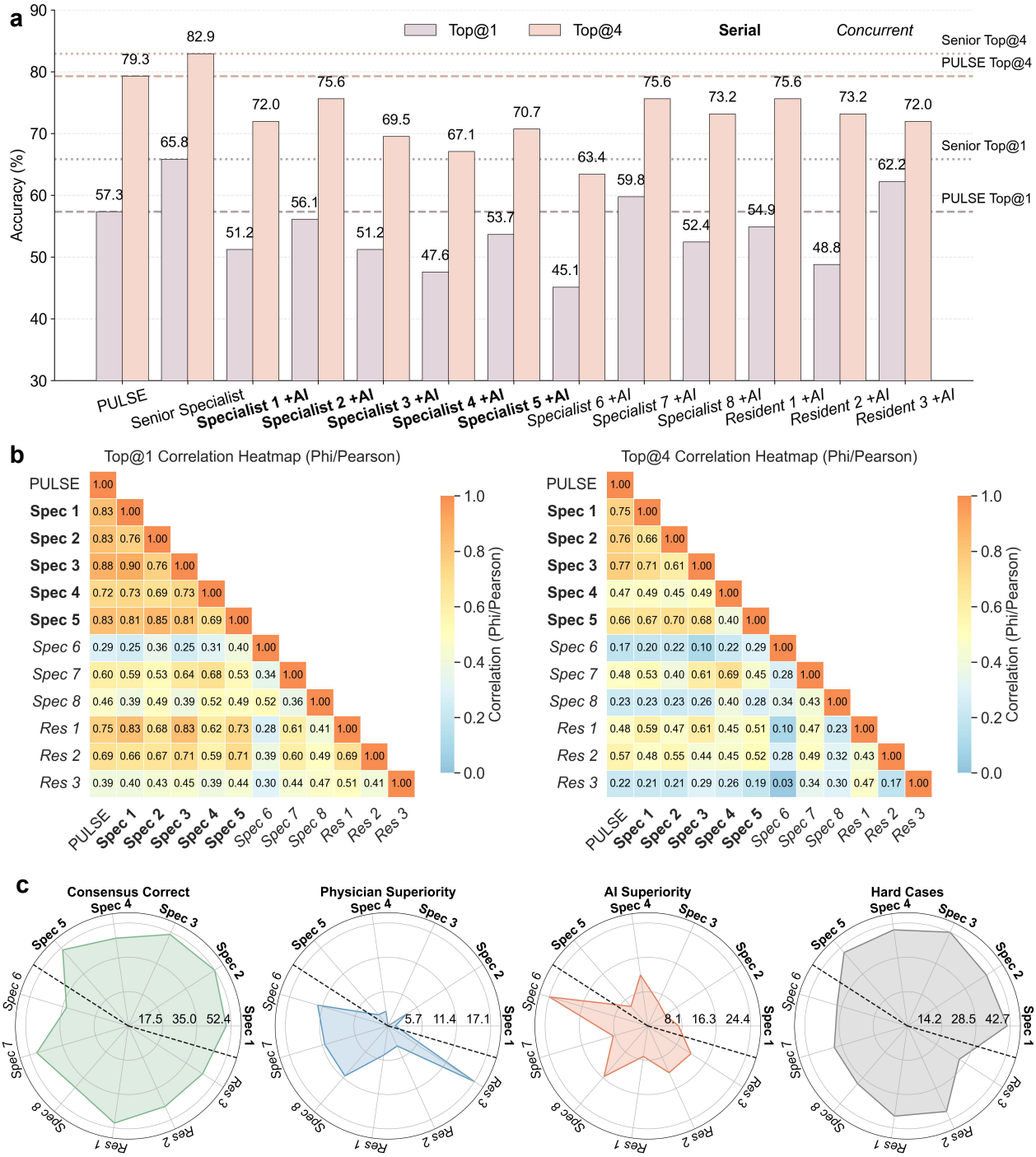

Figure 6: **a**, Diagnostic performance comparison across collaboration workflows. Bar heights represent Top@1 and Top@4 accuracies for physicians assisted by PULSE in serial versus concurrent modes. **b**, Analysis of diagnostic concordance. Heatmaps display pairwise correlation coefficients (Phi/Pearson) between the AI's predictions and the physicians' final decisions for the Top@1 diagnosis (left) and the Top@4 differential list (right). **c**, Radar charts quantify the distribution of cases across four outcome categories: Consensus Correct (both correct), Physician Superiority (physician correct, AI wrong), AI Superiority (AI correct, physician wrong), and Hard Cases (both wrong). Radial axes represent individual physicians, grouped by workflow: serial collaboration (Specialists 1–5, bold labels) and concurrent collaboration (Specialists 6–8 and Residents 1–3, italic labels), separated by dashed boundary lines.

lower unassisted performance—effectively closed the experience gap, achieving Top@1 accuracies of 48.8% to 62.2% and Top@4 accuracies of 72.0% to 75.6%.

Despite similar accuracy gains, the two workflows exhibited markedly different patterns of alignment between AI predictions and physician decisions (Figure 6b). In the serial collaboration group, physicians exhibited high concordance with the agent, with Top@1 correlation coefficients ranging from 0.72 to 0.88 (four of five specialists exceeding 0.80) and Top@4 differential correlations of 0.75 to 0.77. This strong convergence suggests that the subsequent introduction of AI evidence acts as a powerful converging force when physicians first establish an initial diagnostic baseline, leading the physician to either adopt the agent's correct suggestion or reinforce a shared correct judgment. In contrast, physicians who utilized the agent in a concurrent "co-pilot" mode demonstrated significantly lower and more heterogeneous agreement with the AI. Among specialists, Top@1 correlations ranged from 0.29 to 0.60, while residents exhibited the widest variability (0.39–0.75). Importantly, concurrent collaboration exhibited lower AI–physician correlation without sacrificing accuracy (Figure 6b), indicating that high performance in co-pilot mode does not primarily arise from simple adoption of the agent's outputs. Rather, physicians appear to treat the AI as an additional information stream that broadens the hypothesis space while preserving independent judgment.

A direct analysis of the joint outcomes between AI predictions and physician decisions further substantiate this pattern (Figure 6c). In the serial collaboration group, a larger proportion of cases clustered into the consensus correct (45.1%–52.4%) and hard case (39.0%–42.7%) categories, with relatively few misalignments (6.1%–14.6%). By contrast, physicians operating in the concurrent co-pilot mode exhibited substantially more heterogeneous decision shifts. While they surpassed the AI in a higher fraction of cases (3.7%–17.1%), they also underperformed more frequently (7.3%–24.4%), yielding a markedly broader range of misaligned outcomes (12.2%–36.6%).

Collectively, these observations indicate that the structure of human–AI interaction shapes collaborative dynamics. Serial workflows favor convergence and corrective alignment, leveraging prior hypotheses, whereas concurrent workflows preserve autonomy and introduce greater variability, particularly among trainees. This perspective naturally extends the insights from the previous section, linking selective adoption and persistence patterns to the temporal deployment of AI guidance.

Discussion

Complementary strengths of human expertise and AI Our results highlight a fundamental divergence in the mechanisms that underlie diagnostic performance in physicians versus the proposed medical reasoning agent. In this endocrinology case-report set, human accuracy scaled with experience: senior expertise was character-

ized by higher top-1 precision and stronger effort modulation on difficult cases, consistent with more calibrated prioritization under uncertainty. Trainees, in contrast, showed weaker adaptation of deliberation and a narrower working hypothesis space. PULSE showed a different profile. Its accuracy was comparatively stable across incidence tiers and it generated a larger hypothesis space, consistent with access to a broad literature-grounded knowledge base that is not shaped by individual exposure. However, the senior specialist retained an advantage in top-1 specificity, underscoring the importance of contextual gating and nuanced prioritization when converting broad differentials into a single actionable diagnosis. Together, these results support a complementary framing: the agent is well suited for expanding consideration of long-tail diagnoses, whereas expert physicians retain an edge in high-stakes prioritization.

Collaboration dynamics and educational implications How AI is introduced into the diagnostic workflow may be as consequential as the model's standalone accuracy. In our controlled evaluation, both serial and concurrent assistance improved performance relative to unassisted baselines, but benefits depended on physician experience and on how decisions were formed.

In the serial (re-diagnosis) setting, physicians exhibited selective adoption: corrective switches outweighed misleading switches, and correct initial judgments were often preserved. The high correlation between the agent's final outputs and physicians' final decisions suggests that late-stage AI input can act as a strong converging force. This convergence is beneficial when the AI is correct but poses a risk of confirmation bias if trust calibration is poor. In the concurrent setting, agreement between physicians and the agent was lower and more heterogeneous than in serial use, particularly among specialists. Combined with the broader dispersion of joint outcomes, this pattern suggests that early-stage AI support can improve performance without requiring deterministic adoption of model predictions. Practically, concurrent assistance is particularly impactful for less experienced physicians, potentially by expanding the initial hypothesis space before premature closure occurs.

The educational implications are immediate. Rather than viewing AI solely as decision support, it should be conceptualized as an accelerant for competency acquisition. An LLM-based reasoning agent could support exposure to rare and heterogeneous conditions through large volumes of simulated cases with immediate, explainable feedback, thereby accelerating the accrual of illness scripts that typically require years of clinical variety. Emerging simulation paradigms, including AI patient systems, provide plausible vehicles for such curricula [26–28]. Critically, the goal is not to "replace" clinician reasoning, but to shorten time-to-familiarity with uncommon disease presentations while explicitly teaching trainees to interrogate, verify, and appropriately discount AI suggestions.

Case-based archetypes of synergy and discordance Our discordance patterns suggest two clinically intuitive archetypes of complementarity. First, PULSE exhibited a decisive advantage in identifying rare, genetically de-

fined channelopathies and atypical malignancies that trainees systematically missed. Trainee failures were concentrated in conditions that are uncommon, easily confounded with prevalent endocrine syndromes, or require the recognition of biochemical patterns. In cases such as Liddle syndrome and thyroid lymphoma, PUSLE successfully retrieve and prioritize these diagnoses based on subtle biochemical patterns and clinical cues, whereas residents failed to include them in their differentials. These diagnoses share a common educational challenge: they are infrequently encountered yet require disciplined expansion beyond common endocrine "default" syndromes and sensitivity to signature inheritance or biochemical features. Second, physician-correct/AI-incorrect cases exposed a complementary limitation of retrieval-augmented reasoning. A recurring failure mode was bias toward complexity: PULSE scalated to rarer subtypes or mechanistically elaborate explanations without sufficient discriminating evidence (e.g., upgrading familial hypercholesterolemia to homozygous familial hypercholesterolemia). We also observed malignancy anchoring, in which high-salience risk cues (e.g., a mass lesion or severe biochemical derangement) preferentially pulled PULSE toward malignant explanations. For example, immobilization hypercalcaemia could be over-interpreted as malignancy-associated hypercalcaemia, and adrenal-mass contexts sometimes drifted toward high-salience malignant labels when the correct diagnosis was adrenal lymphoma. Collectively, these observations motivate workflow designs that preserve human-led gating while using the agent to broaden early hypothesis generation.

Risks, limitations, and trust calibration Despite the observed utility, LLM-based reasoning agents introduce safety and human-factors risks. LLM-based agents are susceptible to hallucination and can produce fluent rationales that are factually incorrect or poorly aligned with clinical guidelines and workflow constraints [29,30]. Fairness risks remain salient: performance may vary across populations or presentation patterns underrepresented in training data, where the appearance of competence may mask systematic blind spots [31]. Although our study did not directly evaluate subgroup fairness, our collaboration experiments highlight a human-factors risk: physicians can be influenced by incorrect AI suggestions.

Our collaboration experiments further highlight the challenge of trust calibration. Although physicians rarely switched from correct to incorrect diagnoses when the agent erred, we did observe susceptibility to incorrect AI suggestions in a subset of cases—particularly when outputs were presented early and without strong interpretive scaffolding. Conversely, physicians sometimes failed to adopt correct AI suggestions, indicating that assistance is neither uniformly beneficial nor automatically actionable. These bidirectional failure modes support a contingent view in which outcomes depend on workflow design, user expertise, and the legibility and contestability of the agent's reasoning.

One implication is that transparency mechanisms should be treated as core design requirements. Approaches that explicitly separate hypothesis generation from evidence adjudication may help physicians distinguish case-grounded support from background-knowledge extrapolation and better calibrate trust. In parallel,

rigorous evaluation beyond laboratory settings is needed to characterize real-world human–AI interaction effects. Without such safeguards, the breadth that improves rare-disease consideration could introduce spurious distractors, particularly for users with limited ability to critically triage suggestions. Moreover, rigorous fairness evaluation protocols are needed to characterize performance variability and prevent AI assistance from inadvertently widening disparities.

Future directions To translate these findings into clinical practice, future work should prioritize three directions. First, larger-scale randomized controlled studies across multiple institutions are needed to test whether the collaboration effects observed here generalize beyond an endocrinology case-report cohort and to quantify how benefits and risks vary by clinician expertise, case type, and interface design. Second, expanding beyond text-only inputs toward multimodal models that integrate images, laboratory tables, and longitudinal trajectories may better reflect real diagnostic workflows. Third, research should emphasize human–computer interface designs that promote active cognitive engagement—supporting skepticism, structured counterfactual checks, and explicit uncertainty communication—so that AI functions as a reliable and equitable partner rather than a persuasive anchor.

Methods

We introduce PULSE, a medical reasoning agent designed to assist in diagnostic decision-making by integrating a reasoning-oriented LLM with a scientific literature retrieval engine (Figure 7). The framework aims to support healthcare professionals in challenging diagnostic cases by leveraging cutting-edge deep learning techniques alongside the wealth of scientific literature available.

Large languge model The first component of PULSE is a reasoning-oriented LLM, specifically trained for medical reasoning tasks. This LLM is an autoregressive model, composed of multiple decoder-only transformer blocks, optimized for next-token prediction.

Unlike standard LLMs that focus on general language understanding, PULSE's LLM undergoes two stages of fine-tuning on medical data. In the first stage, the model is aligned with foundational medical knowledge through simpler tasks such as medical knowledge question answering, symptom-disease association and medical keyword summarization. These tasks ensure the model gains a solid understanding of clinical concepts and general diagnostic patterns, enabling it to respond to basic queries and provide accurate information on common medical conditions. In the second stage, the model is further refined using carefully curated medical reasoning datasets, which allow it to address more complex clinical reasoning tasks, including differential diagnosis, clinical decision support, and case-based reasoning. This stage enhances the model's ability to handle nuanced clinical cases, integrate evidence, and generate sophisticated diagnostic conclusions.

The model has been trained with 32 billion parameters, utilizing the Qwen3 [25] tokenizer for data processing. The training curriculum covered a total of approximately 10.74 billion tokens. Specifically, the dataset comprised 200 million tokens of medical instruct tuning data and 401 million tokens of medical reasoning data, equipping the model to comprehend a wide range of medical concepts and their interrelationships. This vast parameter scale and targeted dataset enable the LLM to capture subtle patterns and nuances in clinical language, making it particularly effective in generating contextually accurate diagnoses and treatment recommendations based on diverse clinical input.

Framework The PULSE framework functions as a medical reasoning agent designed to assist healthcare professionals in making diagnostic decisions. It integrates a reasoning-oriented LLM with a scientific literature retrieval engine, enabling the system to refine diagnostic conclusions based on both model-generated hypotheses and evidence retrieved from PubMed.

Phase 1: Iterative hypothesis generation. The process begins by diagnosing the clinical case over N rounds. In each round r, the LLM generates a ranked list of n potential diagnoses based on the same input clinical case $\mathcal{C}$. A high temperature setting T_{LLM} is used to encourage exploratory reasoning and diversity. The model outputs a set of n hypothetical diagnoses $\mathcal{H}_r$ at each round r:

$$\mathcal{H}_r = f_{\text{LLM}}(\mathcal{C}, n, T_{\text{LLM}}). \tag{1}$$

Here, $\mathcal{H}_r = \{d_{r,1}, d_{r,2}, \ldots, d_{r,n}\}$ denotes the set of n possible diagnoses generated in round r, and f_{LLM} represents the reasoning LLM.

Phase 2: Diagnosis aggregation. After completing all N rounds, the agent aggregates the diagnoses to identify the most reliable candidates. Since medical concepts can be expressed in various semantically similar ways (e.g., synonyms or slight phrasing variations), simple statistical counting is insufficient. Therefore, the LLM is employed to perform semantic aggregation on the sets $\mathcal{H}_r$ across all rounds. It groups semantically equivalent diagnoses and selects the top m consensus candidates based on their semantic consistency and frequency. This selection process is formulated as:

$$\mathcal{D}_{\text{top}} = f_{\text{LLM}}(\mathcal{H}_1, \mathcal{H}_2, \ldots, \mathcal{H}_N, m), \tag{2}$$

where $\mathcal{D}_{\text{top}} = \{d_1, d_2, \ldots, d_m\}$ is the set of the top m consensus diagnoses. These diagnoses d_i are then used to query PubMed for relevant evidence.

Phase 3: Evidence retrieval. For each disease d_i in $\mathcal{D}_{\text{top}}$, the corresponding evidence articles $\mathcal{E}_i$ are

retrieved from PubMed. The retrieval process is given by:

$$\mathcal{E}_i = \text{PubMedQuery}(d_i), \tag{3}$$

where $\mathcal{E}_i$ represents the set of evidence articles related to disease d_i.

Phase 4: Evidence summarization. Once the evidence is retrieved, the model summarizes the findings relevant to the clinical case $\mathcal{C}$. This summarized information, denoted as $\mathcal{E}_{\text{final}}$, serves as context for the final reasoning,

$$\mathcal{E}_{\text{final}} \leftarrow \text{Summarize}(\mathcal{E}_{\text{all}}, \mathcal{C}). \tag{4}$$

Phase 5: Refined diagnosis. Finally, the LLM generates a refined diagnosis $\mathcal{D}_{\text{final}}$ by considering the clinical case $\mathcal{C}$, the summarized evidence $\mathcal{E}_{\text{final}}$, and the candidate diseases $\mathcal{D}_{\text{top}}$. The final diagnosis is computed as:

$$\mathcal{D}_{\text{final}} = f_{\text{LLM}}(\mathcal{C}, \mathcal{E}_{\text{final}}, \mathcal{D}_{\text{top}}), \tag{5}$$

where $\mathcal{D}_{\text{final}}$ represents the final refined diagnosis. The complete logical flow is summarized in **Algorithm 1**.

Algorithm 1 PULSE Framework: Medical Reasoning with Evidence Retrieval

Require: Clinical Case $\mathcal{C}$, Rounds N, Diagnoses per round n, Top limit m, Temperature T_{LLM}
Ensure: Refined Final Diagnosis $\mathcal{D}_{\text{final}}$

Phase 1: Iterative hypothesis generation
Initialize collection $\mathbb{H} \leftarrow \emptyset$
for round $r \leftarrow 1$ to N **do**
  $\mathcal{H}_r \leftarrow f_{\text{LLM}}(\mathcal{C}, n, T_{\text{LLM}})$ ▷ Generate n diverse diagnoses
  $\mathbb{H} \leftarrow \mathbb{H} \cup \mathcal{H}_r$
Phase 2: Diagnosis aggregation
$\mathcal{D}_{\text{top}} \leftarrow f_{\text{LLM}}(\mathbb{H}, m)$ ▷ Group synonyms & select top m by semantic frequency
Let $\mathcal{D}_{\text{top}} = \{d_1, d_2, \ldots, d_m\}$
Phase 3: Evidence retrieval
Initialize raw evidence set $\mathcal{E}_{\text{all}} \leftarrow \emptyset$
for each disease $d_i \in \mathcal{D}_{\text{top}}$ **do**
  $\mathcal{E}_i \leftarrow \text{PubMedQuery}(d_i)$ ▷ Retrieve relevant articles
  $\mathcal{E}_{\text{all}} \leftarrow \mathcal{E}_{\text{all}} \cup \mathcal{E}_i$
Phase 4: Evidence summarization
$\mathcal{E}_{\text{final}} \leftarrow \text{Summarize}(\mathcal{E}_{\text{all}}, \mathcal{C})$ ▷ Extract findings relevant to $\mathcal{C}$
Phase 5: Refined diagnosis
$\mathcal{D}_{\text{final}} \leftarrow f_{\text{LLM}}(\mathcal{C}, \mathcal{E}_{\text{final}}, \mathcal{D}_{\text{top}})$ ▷ Refine diagnosis with evidence
return $\mathcal{D}_{\text{final}}$

Baselines and experimental benchmarking To strictly evaluate the performance of the PULSE framework, we established comprehensive baselines across both human expertise and state-of-the-art foundation models. The human benchmark cohort was stratified by clinical experience, comprising residents ($n = 8$), junior spe-

cialists ($n = 8$), and a senior attending specialist. We quantified the *experiential capability gap* by analyzing the performance margin between the AI agent and different expertise cohorts, correlating individual diagnostic accuracy (Top@1) with cumulative clinical experience measured in months. For model baselines, we compared PULSE against leading open-weights reasoning models, including gpt-oss-120B [24], Qwen3-235B [25], and DeepSeek-R1 [17]. To rigorously assess robustness, performance was stratified by disease incidence into three tiers: common (0.01–1%), uncommon (0.001–0.01%), and rare ($< 0.001\%$). Additionally, we conducted a granular analysis of model scalability and reasoning effort, comparing performance across model sizes (20B vs. 120B) and explicit reasoning effort settings (low, medium, high).

Model training configuration For the fine-tuning stages, we utilized the AdamW [32] optimizer with $\beta_1 = 0.9$ and $\beta_2 = 0.95$. The learning rate was set to 9×10^{-6} with no warm-up period. To optimize memory efficiency and training throughput, we employed Megatron-LM [33] with a configuration of pipeline parallelism [34] size 2 and tensor parallelism size 8. The batch size was set to 8, with a maximum sequence length extended to $65,536$ tokens utilizing sequence packing. Regularization techniques included a weight decay of 0.1 and a gradient clipping threshold of 1.0 to prevent gradient explosion. The model underwent training for a total of $20,480$ steps.

Framework and inference parameters For the deployment of the PULSE agent, specific hyperparameters were tuned to balance exploration and precision. In the *Iterative hypothesis generation* phase, we set the number of reasoning rounds $N = 8$. To ensure diversity in hypothesis generation, the temperature T_{LLM} was set to 1.0, with a Top-p (nucleus sampling) value of 0.95. For the *Diagnosis Aggregation* phase, the semantic aggregation selected the top $m = 10$ consensus candidates ($\mathcal{D}_{\text{top}}$) for evidence retrieval. In the final *Refined Diagnosis* phase, the temperature was lowered to 0.1 to maximize determinism and factual adherence in the final output.

Retrieval engine specification The scientific literature retrieval engine was built upon the NCBI E-utilities API [35] to access the PubMed database in real-time. The query formulation module converted each diagnosis $d_i \in \mathcal{D}_{\text{top}}$ into a structured boolean query (e.g., combining the disease name with keywords such as "diagnosis", "clinical features", and "case report"). Search results were filtered to prioritize articles published within the last 15 years, ensuring the relevance of medical evidence. For each query, the top $k = 20$ abstracts were retrieved. To address context window limitations and ensuring case-specificity, we employed the LLM itself for the summarization step. The model was prompted to read the raw retrieved abstracts $\mathcal{E}_{\text{all}}$ alongside the clinical case $\mathcal{C}$, extracting and synthesizing only the findings directly relevant to the patient's presentation. This LLM-generated summary formed the concise evidence context $\mathcal{E}_{\text{final}}$ used for the final diagnostic reasoning.

Computing Software and Hardware All experiments were conducted using Python (version 3.10). The PULSE large language model (LLM) was implemented using the PyTorch deep learning framework (version 2.8.0) and trained using Megatron-LM (version 250908) for large-scale distributed training. Model training was performed on a high-performance computing cluster equipped with 16× NVIDIA H100 GPUs (80GB memory each) with CUDA-enabled acceleration. Data processing and statistical analyses were conducted using NumPy (version 2.2.6), SciPy (version 1.15.3), Pandas (version 2.3.3), and Statsmodels (version 0.14.6). Figures and visualizations were generated using Matplotlib (version 3.10.7) and Seaborn (version 0.13.2).

Data availability The clinical dataset used in this study comprises 82 real-world endocrinology cases curated from authentic clinical records. Owing to patient privacy and institutional data protection regulations, these data are not publicly available. All records were strictly de-identified prior to use to remove personally identifiable information (PII) in accordance with applicable ethical and regulatory standards. The dataset includes cases spanning multiple endocrine disease categories—including adrenal, pituitary, thyroid, parathyroid and neuroendocrine disorders—with ground-truth diagnoses verified by definitive biochemical assays, histopathological examination or genetic testing. To simulate real-world diagnostic conditions, only information available at the initial clinical encounter (including history of present illness, physical examination findings and initial laboratory or imaging results) was provided for model evaluation. Access to the de-identified dataset may be granted for academic research purposes upon reasonable request to the corresponding author, subject to institutional approval and data-sharing agreements that ensure compliance with patient privacy and data protection regulations.

Code availability Reviewers were provided access to an LLM-based chat system for evaluation purposes during peer review. The model weights underlying the PULSE system are not publicly released due to the potential safety risks associated with the unmonitored deployment of clinical decision-support models. To promote responsible development and prevent inappropriate use in medical settings without adequate clinical oversight, access to the full implementation is currently restricted. To facilitate reproducibility and transparency, the key methodological components and model architecture are described in detail in the Methods section. The framework code is available at `https://github.com/SPIRAL-MED/PULSE`. And Researchers interested in evaluating the PULSE system may request access through the publicly available PULSE API. Access may be granted for research purposes subject to review and compliance with relevant use policies.

Author contributions Z.Z.H. and L.J.M. wrote the manuscript. Y.L., H.C., Y.F. and L.X.M. conceived the study and designed the experiments. Y.L., H.C., Y.F. and L.W. performed data collection and processing. Z.Z.H., L.J.M. and X.F.Z. developed the model. Y.L., H.C., Y.F., X.F.Z. and L.X.M. conducted experimental analysis and interpreted the results. X.F.Z. and L.X.M. reviewed and revised the manuscript. S.T.Z. and K.Q. supervised the research.

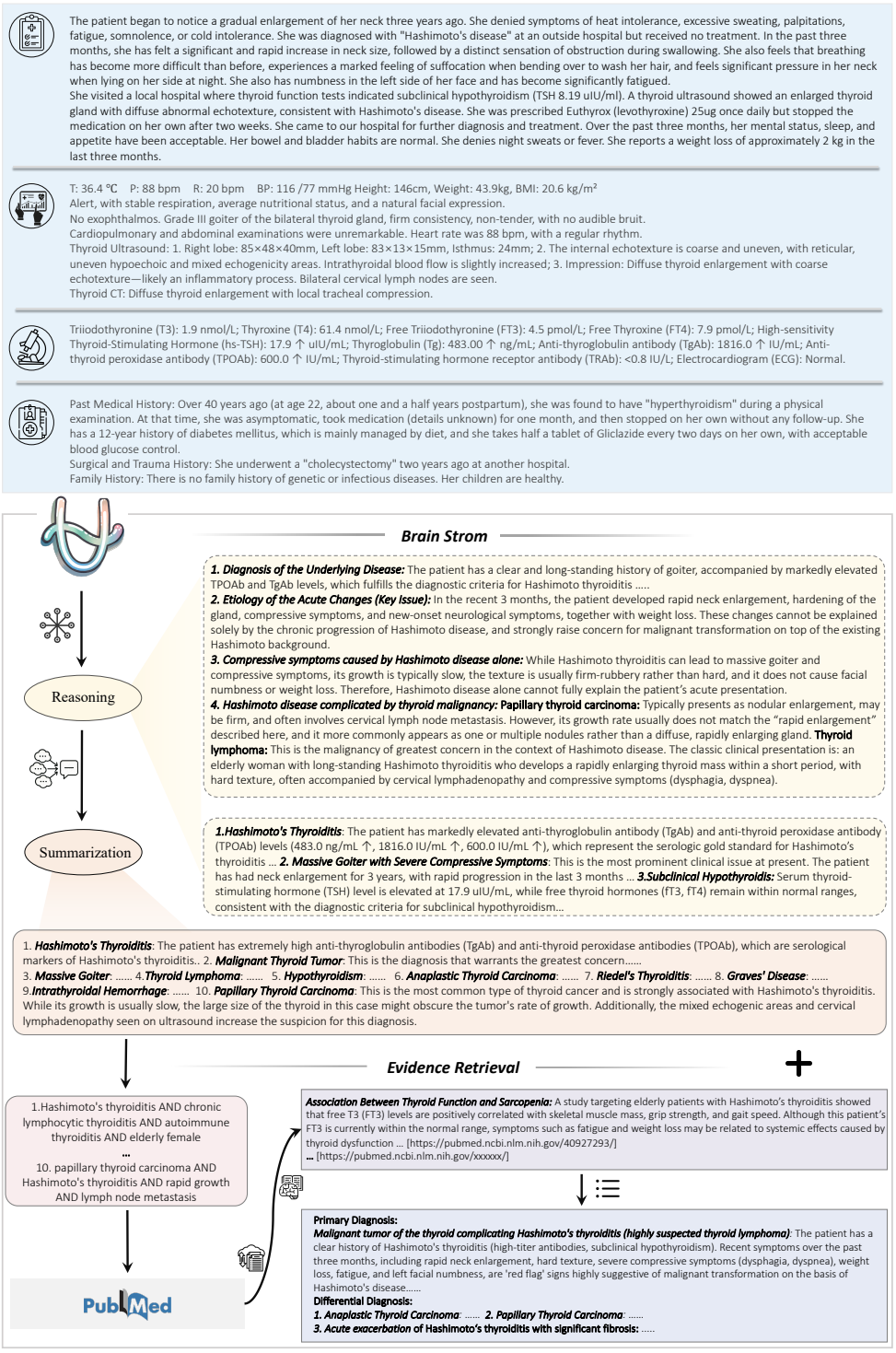

Figure 7: **a**, The workflow begins with the structured ingestion of comprehensive clinical information, including patient history, physical examination findings, and laboratory data. **b**, The LLM performs iterative hypothesis generation ("brainstorming") and abstraction, distilling salient features—such as rapid cervical enlargement and elevated thyroid autoantibodies—to generate a spectrum of plausible aetiologies. **c**, High-priority diagnostic hypotheses are subsequently subjected to targeted evidence retrieval from PubMed to interrogate specific clinicopathological associations (for example, the link between Hashimoto's thyroiditis and lymphoid malignancy). **d**, Finally, the agent synthesizes model-derived clinical reasoning with retrieved scientific evidence to arrive at a definitive primary diagnosis (malignant lymphoma arising in the context of Hashimoto's thyroiditis) and a ranked differential diagnosis.

References

1. Moor, M. *et al.* Foundation models for generalist medical artificial intelligence. *Nature* **616**, 259–265 (2023).

2. Auerbach, A. D. *et al.* Diagnostic errors in hospitalized adults who died or were transferred to intensive care. *JAMA Internal Medicine* **184**, 164–173 (2024).

3. Lin, M. P. *et al.* Potential diagnostic error for emergency conditions, mortality, and healthy days at home. *JAMA Network Open* **8**, e2516400–e2516400 (2025).

4. Marwaha, S., Knowles, J. W. & Ashley, E. A. A guide for the diagnosis of rare and undiagnosed disease: beyond the exome. *Genome medicine* **14**, 23 (2022).

5. Limongelli, G. *et al.* Argo delphi consensus statement on red flags and clinical gateways towards rare disease diagnosis. *Scientific Reports* **15**, 39411 (2025).

6. Neumann, H. P., Young Jr, W. F. & Eng, C. Pheochromocytoma and paraganglioma. *New England journal of medicine* **381**, 552–565 (2019).

7. Casey, R. T. *et al.* International consensus statement on the diagnosis and management of phaeochromocytoma and paraganglioma in children and adolescents. *Nature Reviews Endocrinology* **20**, 729–748 (2024).

8. Tu, T. *et al.* Towards conversational diagnostic artificial intelligence. *Nature* 1–9 (2025).

9. El-Kareh, R. & Sittig, D. F. Enhancing diagnosis through technology: decision support, artificial intelligence, and beyond. *Critical care clinics* **38**, 129 (2022).

10. Ball, J. R., Miller, B. T. & Balogh, E. P. Improving diagnosis in health care (2015).

11. Newman-Toker, D. E. *et al.* Burden of serious harms from diagnostic error in the usa. *BMJ Quality & Safety* **33**, 109–120 (2024).

12. Thirunavukarasu, A. J. *et al.* Large language models in medicine. *Nature medicine* **29**, 1930–1940 (2023).

13. Giorgini, F., Di Dalmazi, G. & Diciotti, S. Artificial intelligence in endocrinology: a comprehensive review. *Journal of endocrinological investigation* **47**, 1067–1082 (2024).

14. Funder, J. W. *et al.* The management of primary aldosteronism: case detection, diagnosis, and treatment: an endocrine society clinical practice guideline. *The Journal of Clinical Endocrinology & Metabolism* **101**, 1889–1916 (2016).

15. Yu, J. Endocrine disorders and the neurologic manifestations. *Annals of Pediatric Endocrinology & Metabolism* **19**, 184 (2014).

16. Jaech, A. *et al.* Openai o1 system card. Tech. Rep. (2024).

17. Guo, D. *et al.* Deepseek-r1 incentivizes reasoning in llms through reinforcement learning. *Nature* **645**, 633–638 (2025).

18. Gibney, E. Scientists flock to deepseek: how they're using the blockbuster ai model. *Nature* (2025).

19. Gaube, S. *et al.* Non-task expert physicians benefit from correct explainable ai advice when reviewing x-rays. *Scientific reports* **13**, 1383 (2023).

20. Tang, H. *et al.* Ai-assisted diagnosis and decision-making method in developing countries for osteosarcoma. In *Healthcare*, vol. 10, 2313 (MDPI, 2022).

21. Lu, C., Zhang, J. & Liu, R. Deep learning-based image classification for integrating pathology and radiology in ai-assisted medical imaging. *Scientific Reports* **15**, 27029 (2025).

22. Acosta, J. N., Falcone, G. J., Rajpurkar, P. & Topol, E. J. Multimodal biomedical ai. *Nature medicine* **28**, 1773–1784 (2022).

23. OpenAI. Gpt-5.1: A smarter, more conversational chatgpt. `https://openai.com/index/gpt-5-1` (2025).

24. Agarwal, S. *et al.* gpt-oss-120b & gpt-oss-20b model card. *arXiv preprint arXiv:2508.10925* (2025).

25. Yang, A. *et al.* Qwen3 technical report. *arXiv preprint arXiv:2505.09388* (2025).

26. Yu, H. *et al.* Simulated patient systems powered by large language model-based ai agents offer potential for transforming medical education. *Communications Medicine* (2025).

27. Zeng, J. *et al.* Embracing the future of medical education with large language model–based virtual patients: Scoping review. *Journal of Medical Internet Research* **27**, e79091 (2025).

28. Elhilali, A., Ngo, A. S.-H., Reichenpfader, D. & Denecke, K. Large language model–based patient simulation to foster communication skills in health care professionals: User-centered development and usability study. *JMIR medical education* **11**, e81271 (2025).

29. Huang, L. *et al.* A survey on hallucination in large language models: Principles, taxonomy, challenges, and open questions. *ACM Transactions on Information Systems* **43**, 1–55 (2025).

30. Farquhar, S., Kossen, J., Kuhn, L. & Gal, Y. Detecting hallucinations in large language models using semantic entropy. *Nature* **630**, 625–630 (2024).

31. Zack, T. *et al.* Assessing the potential of gpt-4 to perpetuate racial and gender biases in health care: a model evaluation study. *The Lancet Digital Health* **6**, e12–e22 (2024).

32. Loshchilov, I. & Hutter, F. Decoupled weight decay regularization. In *Proceedings of the International Conference on Learning Representations* (2019).

33. Shoeybi, M. *et al.* Megatron-lm: Training multi-billion parameter language models using model parallelism. *arXiv preprint arXiv:1909.08053* (2019).

34. Narayanan, D. *et al.* Efficient large-scale language model training on gpu clusters using megatron-lm. In *Proceedings of the International Conference for High Performance Computing, Networking, Storage and Analysis*, 1–15 (2021).

35. Sayers, E. A general introduction to the e-utilities. *Entrez Programming Utilities Help [Internet]. Bethesda (MD): National Center for Biotechnology Information (US)* (2010).